

Article

# Interface Characterization of Ultrasonic Spot-Welded Mg Alloy Interlayered with Cu Coating

Amir Badamian <sup>1,\*</sup>, Chihiro Iwamoto <sup>2</sup>, Shigeo Sato <sup>2</sup> and Suguru Tashiro <sup>2</sup><sup>1</sup> Graduate school of science and engineering, Ibaraki University, Hitachi, Ibaraki 316-8511, Japan<sup>2</sup> Department of Materials Science and Engineering, Ibaraki University, Hitachi, Ibaraki 316-8511, Japan; chihiro.iwamoto.77@vc.ibaraki.ac.jp (C.I.); shigeo.sato.ar@vc.ibaraki.ac.jp (S.S.); suguru.tashiro.5045@vc.ibaraki.ac.jp (S.T.)

\* Correspondence: amir\_badamian@yahoo.co.jp

Received: 8 April 2019; Accepted: 5 May 2019; Published: 8 May 2019



**Abstract:** The effect of Cu coating metallic interlayer on the weldability, joint strength, and interfacial microstructure during high-power ultrasonic spot welding (HP-USW) of AZ31B Mg alloy has been studied. Interlayered samples exhibited good weldability and they resulted in strong sound joints with nearly the same strength as joints without interlayer, with the distinction of lower energy being required. The Cu interlayer affected the thermal and vibrational properties of the interface, as the maximum interface temperature decreased and approached better uniformity across the weld nugget. The base metal grain structure changed to equiaxed larger grains after ultrasonic welding and a chain of parent metal small grains were observed around the interface. A binary intermetallic compound product of Mg-Cu, which was rich in Mg, has been found around the interface that was diffused toward base metal. According to the electron probe micro-analyzer (EPMA) results, alongside temperature measurements and hardness data, the formation of Mg<sub>2</sub>Cu is suggested in this region. At the interface centerline, a narrow region was identified that was composed of Mg, Cu, and Al. Complementary transmission electron microscopy analysis estimated that Al-containing reaction product is a ternary alloy of the MgCu<sub>x</sub>Al<sub>y</sub> type. The dispersion of fine grain intermetallic compounds as discrete particles inside Mg substrate in both interfacial regions formed a composite like structure that could participate in joint strengthening.

**Keywords:** high-power ultrasonic welding; interface; magnesium; cu interlayer; intermetallic compound

## 1. Introduction

Mg alloys are increasing in demand due to their high specific strength (strength to density ratio) and they have attractive applications in automotive industries, aerospace, medical implants, electronic appliances, and sport equipment [1,2]. Different methods are available for the joining of magnesium alloys. The primary methods include tungsten arc welding (TIG), laser beam welding (LBW), resistance spot welding (RSW), electromagnetic welding (EMW), electron beam welding (EBW), diffusion bonding, soldering, brazing, adhesive bonding, and mechanical fastening. Fusion based welding methods, like TIG, LBW, RSW, etc., have major problems that are mostly related to low boiling temperature of magnesium alloys that leads to porosities and hot cracking in the weld line and heat affected zone (HAZ). The other main limitations include high energy consumption and the need of consumables [3,4]. Therefore, the development of solid-state processes, like friction stir welding (FSW), friction stir spot welding (FSSW), and ultrasonic spot welding (USW) helped to avoid problems that are related to melting and provide opportunities for dissimilar material welding [5–7]. However, FSW and FSSW have the limitations of making “keyhole” and the need to fixture and a long process time [5].

USW is considered to be a solid-state welding process, with low energy consumption and time saving process and no need for consumables or atmosphere control. It is using relatively high frequency ultrasonic vibrations (20–40 KHz) that induce the workpieces to be held together with simultaneous pressure, which leads to frictional shear forces parallel to the interface. Under the effect of frictional shear forces, surface oxide layers break down and two joining parts approach bare contact and the temperature increases due to friction, and then local welding occurs between the asperities of two faying surfaces. Finally, the spreading of local micro-welds and coalescence results in the creation of a metallurgical bond in the weld spot [5,7–11].

High-power ultrasonic spot welding (HP-USW) is an effective way of achieving sound strong joints among different USW methods. This method uses higher power and lower energy and time when compared to other spot-welding processes [12]. The use of high energy levels (or equally longer welding times) may cause extra-thinning of the joint and induce cracks in the weld nugget that limits access to maximum joint strength [9]. Furthermore, the use of interlayer in USW mostly related to weldability improvement, especially in dissimilar joining. Typically, use of metallic foil interlayer is more convenient and cost effective than other methods, like sputtering, plating, etc. [8]. The first trials of current research also performed using Cu foil in different thicknesses and USW energies. However, those experiments resulted in relatively strong joints, but the use of Cu coating was more effective in achieving better weldability and mechanical properties.

According to authors knowledge and a review on previous research studies, the use of Cu as an interlayer in the AZ31B Mg alloy “similar USW” has not been recorded. Previous efforts mostly were related to processes other than USW, the same as TLP (transient liquid phase), eutectic, or diffusion bonding. HP-USW of AZ31 Mg alloy classifies similar joining, but, when Cu used as an interlayer in contact with Mg, it forms a dissimilar welding combination at the interface. Hence, it is beneficial to review the Mg-Cu bonding processes and diffusion behavior, as well as AZ31 that is interlayered with Cu through other processes to find out the possible interactions in this system.

Diffusion kinetics and the identification of interfacial layers between Mg and Cu (pure metals) were studied by Nonaka et al. [13] and they reported the formation of  $Mg_2Cu$  as major interfacial layer near Mg and a thin layer of  $MgCu_2$  adjacent to Cu (410–475 °C). Additionally, they suggested that the diffusion of Cu in Mg is faster than the inverse. However, in a nearly same recent study by Dai et al. [14], there was agreement about formation of two intermetallic layers between Mg and Cu, but they reported a different interdiffusion priority based on measured diffusion coefficients and activation energy data. These are basic studies regarding the Mg-Cu reaction diffusion couple, but, in the field of ultrasonic welding, Macwan and Chen [15] applied HP-USW for joining AZ31 to Cu (2000 W, 1000–2500 J) and observed the formation of a diffusion layer around the interface containing Mg +  $Mg_2Cu$  that spread just towards the Mg side. They proposed a mechanism that is mainly based on the preferable diffusion of Cu in Mg to form  $Mg_2Cu$  intermetallic compound besides liquid phase formation through the eutectic reaction. This behavior was mostly attributed to the differences in the physical properties between Cu and Mg, such as melting point, thermal conductivity, heat capacity, and atomic radius.

One of trials to use the Cu interlayer was related to the field of eutectic bonding, where Elthalabawy et al. [16,17] studied joining AZ31 to 316L steel using a Cu insert (at 530 °C), and found that the eutectic reaction between Mg and Cu after 1 min. resulted to formation of 4 distinct interfacial layers in Mg part. Middle interfacial layers included  $Mg_2Cu$  and a layer of ternary Mg + Cu + Al composition wherein Al content depleted from AZ31 base metal to participate in the Al-containing product.

The participation of AZ31 alloying elements in interfacial phenomena makes it more complicated, which can lead to non-stoichiometric compositions. Anyway, the formation of intermetallic compound (IMC) reaction products in dissimilar joining is prevalent and, in most cases, it has negative effect on mechanical properties of the joint, because they can embrittle the interface, especially when a continuous layer formed. Panteli et al. [18–20], during HP-USW of AZ31 to Al-6111, observed a 5  $\mu m$  thickness continuous IMC layer along the interface, which resulted in low tensile shear strength with

interfacial fracture. Additionally, they found that, under dynamic high strain rates of USW, the rate of IMC product formation was twice when compared to normal static conditions [18–20]. Patel et al. [21,22] also used HP-USW to join AZ31-Al 5754 and AZ31-HSLA steel combinations while applying a 50  $\mu\text{m}$  thickness Sn interlayer and, finally, the Sn interlayer improved the weld strength in lower energies. The improvement was attributed to the formation of a composite-like Sn +  $\text{Mg}_2\text{Sn}$  eutectic structure instead of forming a brittle IMC product without an interlayer.

The objective of the current research is to study the effects of using a Cu coating interlayer in HP-USW of AZ31B Mg alloy on the weldability, mechanical strength, and process optimization from the point of view of energy, time, and interface characterization.

## 2. Materials and Methods

Commercial AZ31B rolled plates of magnesium alloy (3%Al, 1%Zn in wt%) with dimensions of 50 mm in length, 20 mm in width, and thickness of 0.8 mm were used as the initial material. The plates faying surfaces were polished until #2000 by emery paper, and finally cleaned while using acetone prior to USW. Final polishing resulted in a decrease of plate thickness, hence the applicable plate thickness was 0.78 mm. Joint welding carried out using a 2500 W, 20 KHz single wedge-reed USW machine MH2026/CLF2500 that was equipped with weld control monitoring system TDM-10AC (TMEIC/SONOMAC JAPAN Inc. Yokohama, Japan). Figure 1 presents a schematic of this machine. Additionally, a real photo of the sonotrode tip, as shown in Figure 1b (up), which has a circular shape with special design of two surfaces, including: “flat region” and “slope region”. The flat region of tip head surface (5 mm in diameter) serrated with a knurling pattern that consisted of  $14 \times 14$  rows of indentations (see a magnified view in Figure 1b; down), which can help to better the friction and plastic deformation on the weldment.

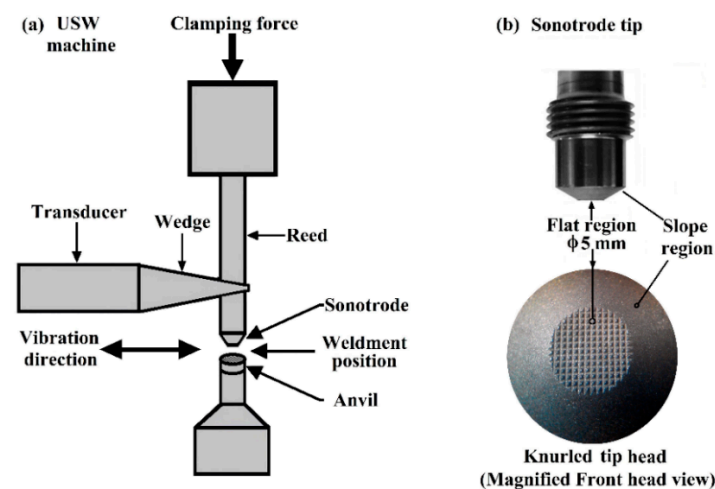


**Figure 1.** (a) Schematic of single wedge-reed type ultrasonic spot welding (USW) machine used in current research; (b) sonotrode tip head (up: side view; down: Magnified normal view of head surface).

An overlap of 20 mm  $\times$  20 mm between two plates was considered in order to perform lap shear tensile test on welded samples and, in order to prevent rotation of plates under effect of ultrasonic vibrations, the plates were kept together prior to welding using slight pressing on two points near the tip affecting area. A schematic representation of the welded sample for lap shear tensile testing and/or microstructure analysis is shown in Figure 2a. Additionally, Figure 2b shows a typical macrography of the welded joint intersection including Cu interlayer.

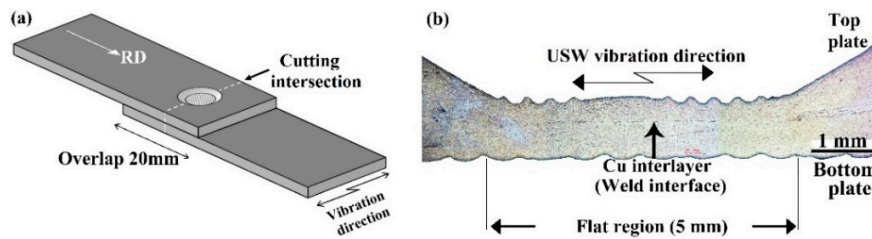


**Figure 2.** (a) Schematic of welded sample; (b) typical welded joint intersection (RD: Rolling direction).

Lap shear tensile tests on the welded specimens were performed using 0.5 ton-f, DS-3100 (Showa inc., Tokyo, Japan) desk type tensile machine under 1mm/min. cross head speed. The tensile axis was along the length of plates (i.e., perpendicular to vibration direction). For hardness evaluations, an MVK-H1 microhardness testing machine (AKASHI inc., Yokohama, Japan) used according to ASTM E-384-2011. A hardness measurement for welded samples has been conducted inside the flat region.

From the point of view of using or not using interlayer, two types of USW joints were produced, including:

- Joint type A: Direct welding of AZ31B plates without using interlayer; and,
- Joint type B: Cu coated AZ31B top plate welded to uncoated AZ31B bottom plate.

The high-power of 2450W was selected as the maximum capability of USW machine that was allowed by maker under safe conditions. USW parameters (same as impedance and clamping pressure) were optimized to access the maximum mechanical strength for all series of joints. Since that impedance is a variable that changes under different conditions of weldments, like coatings, oxide layers, or machine related design, it should be optimized under the maker's instructions before experiments. Subsequently, pressure optimization has been done under optimized impedance and a desired medium constant energy (e.g., 1500 J energy for joint type A and 1000 J for joint type B). Finally, the main experiments were performed under the optimized obtained pressure of 0.56 MPa for both joint types. The range of applied energy was selected between 800–1600 J, which covers low to high levels of energy and it has been monitored test by test according to lap shear tensile test results. The welding time and tip penetration depth were dependent variables that changed with change of energy. Ultrasonic vibration direction was along the plate width, perpendicular to rolling direction (RD) (see Figure 2a,b). The welded samples were cut from the width intersection (parallel to the vibration direction) for microstructure evaluations, including light microscopy, scanning electron microscopy (SEM) and electron backscatter diffraction analysis (EBSD) by SU5000 (Hitachi high-Technologies Ltd., Hitachi, Japan), electron probe micro-analyzer (EPMA) JXA8200T (JEOL Ltd., Tokyo, Japan), and transmission electron microscopy (TEM) analysis by JEM-2010 (JEOL Ltd., Tokyo, Japan). TEM sample cutting was performed using low speed diamond saw blades and polishing was continued until 0.5  $\mu\text{m}$  (60000 grit) with abrasive polishing paper and finally dimpled with GATAN 656 and PIPS-GATAN 691 (Gatan Inc., Pleasanton, CA, USA). Oil-based diamond slurry was used for the final polishing of light microscopy and SEM-EBSD samples, to prevent oxidative corrosion. For a revealing microstructure with light microscopy, acetic-picral etchant was used, which is a common etchant that is capable of revealing Mg grain boundaries. Mean grain size measurement has been performed with using the line intercept method. Final polishing was continued with ion milling by HITACHI IM-4000 series (Hitachi high-Technologies Ltd., Hitachi, Japan) for EBSD and EPMA analysis.

Cu interlayer was deposited through the vacuum vapor deposition method. Deposition was applied just on the overlapping contact area (20 mm  $\times$  20 mm) of the AZ31B top plate.

A notch was created at the center part of bottom plate overlap surface for temperature measurements, as shown in Figure 3, and a 0.5 mm K-type thermocouple was inserted inside the notch to near the center of the weld nugget surface.

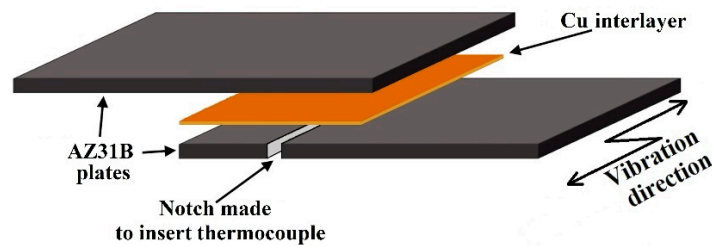


Figure 3. Schematic configuration for temperature measurement.

### 3. Results and Discussion

#### 3.1. Lap Shear Tensile Test Results

Figure 4 shows a comparative graph of maximum lap shear tensile force for two types of samples in different energy levels. All of the tests were optimized to use 0.56 MPa clamping pressure. Each data in the curve is the average of three samples.

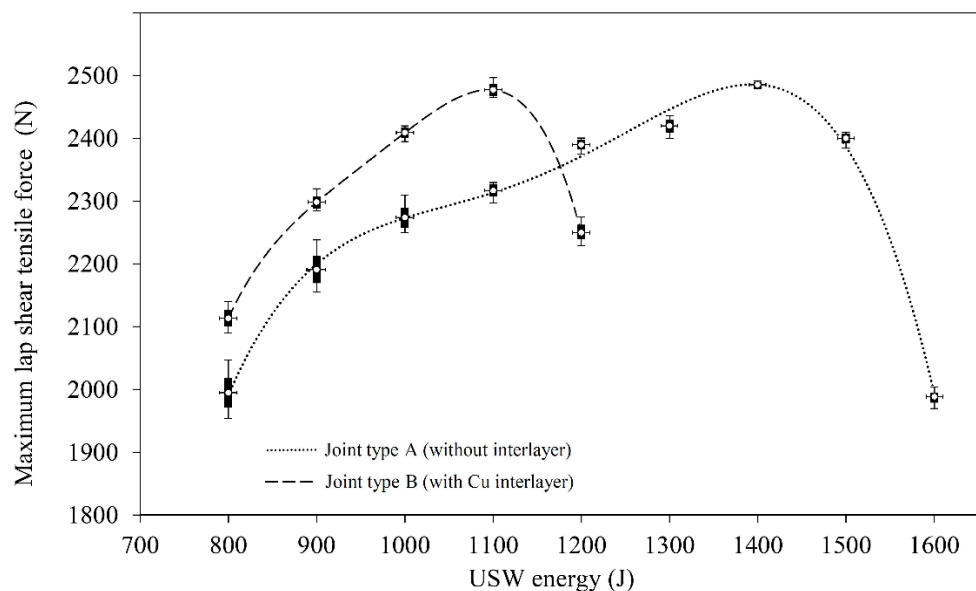
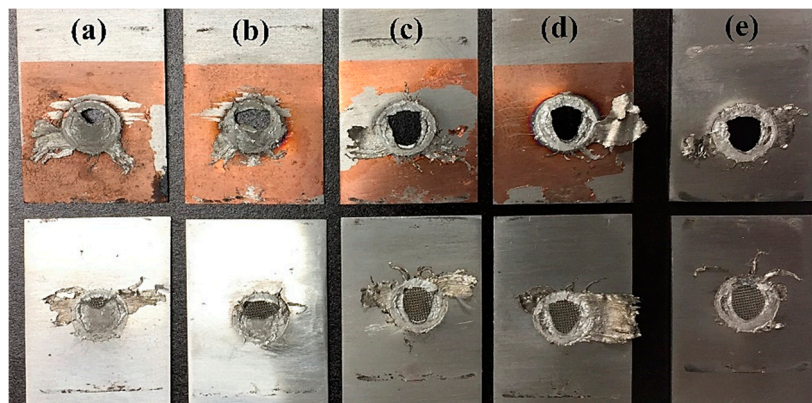


Figure 4. Comparative lap shear tensile force data vs energy, in high-power ultrasonic spot welding (HP-USW) of AZ31B, with and without interlayer (A: without interlayer; B: using Cu coating as interlayer).

The average maximum force that was achieved with joint type A, was 2485 N, while, in the case of joint type B, it was 2477 N, which is comparable with type A, but the used energy to achieve peak point for interlayered joint of type B was 20% lower, being equal to 1100 J. There were some cases that the maximum force data of joint type B was higher than that for joint type A, or the failure occurred in the base metal (out of weld spot).

The presented curves in Figure 4 imply that after a certain amount of applied USW energy, in both series of samples, with increasing USW energy, the curves reached a maximum and higher levels of used energy resulted in a relatively sharp drop in the maximum lap shear tensile force. For a better understanding of this effect, a macrography of failed samples after lap shear tensile testing is shown in Figure 5, which correlates change in failure behavior with USW energy. Figure 5a–d are related to the joint type B samples in energies of 900, 1000, 1100, and 1200 J respectively. Figure 5e that is related to the strongest sample of joint type A (1400 J) is presented to compare with 5c (strongest sample among joint type B).



**Figure 5.** Failed samples after lap shear tensile testing for joint type B at (a) 900 J; (b) 1000 J; (c) 1100 J; (d); 1200 J; and, (e) joint type A at 1400 J USW energy.

The full nugget pull-out in samples of joint type B occurred when higher USW energies were applied ( $\geq 1100$  J), while in lower USW energies ( $< 1100$  J), weld button was partly pulled out like a mix of pull out and the interfacial shear fracture. Hence, partial pull-out gradually changed to a complete pull-out of weld button, which is correspondent with the data attained in the related graph in Figure 4. With a comparison between the strongest samples of both joint types (Figure 5c,e), it can be found that the Cu-interlayered sample and the sample without interlayer mostly showed the same failure behavior.

The relationship between different parameters of USW is not simple and the main parameters are energy, power, and clamping force (pressure), and other parameters can be assumed as the dependent parameters like welding time or tip penetration depth that change with changing of energy. There is a famous relationship between power, energy, and time, as that energy equals to the multiplication of power and time. However, according to current research results and many other HP-USW studies, it can be found that this relationship is not completely responsible in HP-USW. For example, in the welding conditions of 2450 W and 800 J energy, the recorded welding time was 0.7 s, while, according to the energy-power relationship, it should be around 0.33 s. The other point is the role of clamping force, which is normally used to establish a continuous intimate contact between two plates during USW. Logically, it can be considered that with an increasing of clamping force, a preventive force is working opposite to frictional force, which can result in the prohibition of easy movement between two joining parts. However, the application of HP-USW results in the need of increased higher clamping forces to keep the weldments together. Liu et al. [23], who studied the vibration amplitude effects on ultrasonic welding of Cu-Al joints, also noticed that interactions between different USW parameters have great influence on the mechanical performance of the joints, however a moderate clamping force is indispensable in generating intimate contact between the welded samples, and high power levels are required for extensive deformation that is associated with high clamping force.

Energy is one of the more attentional parameters in USW. Generally, USW energy can influence final strength in different ways comprising an increase in sonotrode tip penetration depth (or decreasing the joint thickness as a result), expanding the weld nugget surface area, and raising the temperature or heat delivered to the weldment. In lower energies, the produced frictional heat is not enough to bring the interface temperature up to levels that are necessary for completely occurring interfacial phenomena, like diffusion, eutectic reaction, etc. In other words, in lower energy levels, if IMC's formed at the interface during USW, they cannot diffuse and distribute correctly in the base metal and may play a role of imperfection at the interface that attenuates joint strength, because of less energy and inadequate heat input.

On the other side, when the applied energy is more than that needed to achieve a perfect joint (such as energies  $> 1100$  J in joint type B), it can lead to an increase in the maximum interface temperature and extra melting possibly occurs at the interface layer, which encounters the highest rate of temperature

rise. Thermochemistry data available for Mg-Cu intermetallic system implies that the formation of both IMC products in this system ( $Mg_2Cu$  and  $MgCu_2$ ) is exothermic due to the negative enthalpy of formation [24]. It means that generated heat in these exothermic reactions may assist in temperature rising, however in small amounts. Consequently, if significant amounts of liquid phase are present at the interface, the rapid cooling after USW may result in brittle solidified reaction products, especially near the nugget edge walls. Several researchers reported the occurrence of melting during the use of interlayer, especially at the nugget edge walls. In recent research by Peng et al. [25] for dissimilar USW of Mg-ZEK100 to Al-6022 while using a 50  $\mu m$  Cu interlayer, they reported locally melting at the nugget edges that were attributed to the high stress concentration that caused increase in temperature and lead to molten eutectic reaction products of  $Mg + Mg_2Cu$ , which were squeezed in nugget edges that resulted in interfacial fracture. The same evidence was observed with Macwan for HP-USW of Mg to Cu, and in high levels of USW energy (1500 J) the diffusion eutectic layer was squeezed out of the nugget edge [15,26]. Some melting at the nugget edge walls were rather visible, as it can be found in a higher energy sample of Figure 5d. The pulled-out weld button has a rather smaller area when compared to 5c, which is evidence of the high energy effect.

In the other hand, higher energy effects on joint thickness and it results in the thinning of the joint, thereupon introducing more stress concentration, leading to crack initiation in the weld nugget. Other researchers have frequently reported this behavior. For example, Peng et al. [27], during HP-USW of Al-6022, achieved the maximum mechanical strength at the intermediate energies of 1200–1400 J and the final strength was decreased by increasing the energy to higher levels, hence they attributed this to crack growth and stress concentration that were caused by deeper tip penetration. The measured average joint thickness for A and B joint types showed that total weldment initial thickness of 1.56 mm before USW (2 mm  $\times$  0.78 mm), was decreased to about 0.81 mm for joint A (1400 J energy) after HP-USW, while, in the case of type B, which used the Cu interlayer and made in lower energy of 1100 J, the final joint thickness was 0.95 mm. This can be found from Figure 6a,b in a critical region at the end of interface flat part that continues with the slope region.

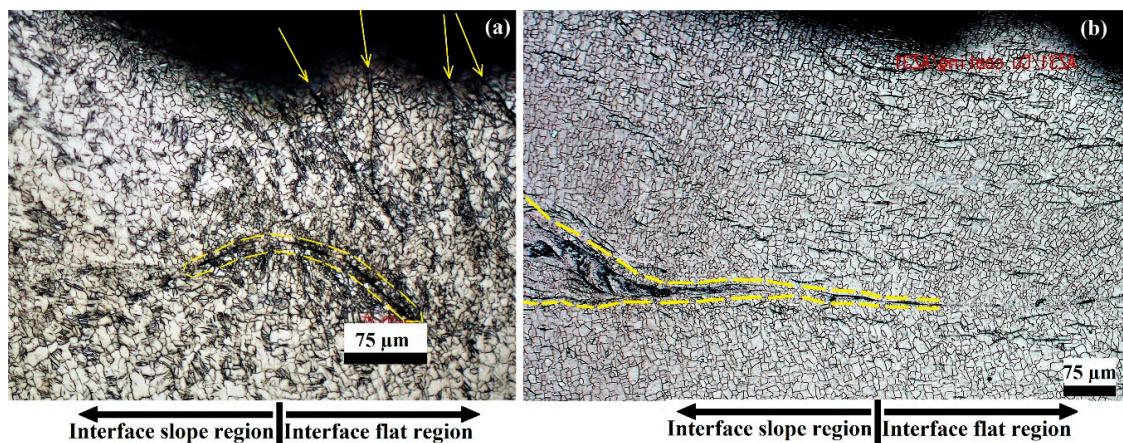


**Figure 6.** Comparison between macrographs of joint type A and B in transition region from flat part to slope part of the interface; (a) Joint type A (1400 J); (b) joint type B (1100 J).

In Figure 6a, which is related to joint type A, the arrow markers are notifying some cracks near the slope region that are introduced due to high energy and deep penetration of the sonotrode tip, resulting in extra thinning of joint thickness, especially in the top plate. Moreover, the region in Figure 6a that is confined within dashed lines shows a transitional region between the flat and slope part, with extreme plastic deformation and flow, which led to discontinuity in nugget edges under the effect of higher energy levels. Opposite to Figure 6b, when using the Cu coating interlayer, the joint thickness improved under lower energy USW, followed with an appearance of low melting point IMC products in a transitional region from flat to the slope part of interface (marked within a dashed

line area). In comparison with Figure 6a, cracks cannot be seen in similar area. However, in this case, severe difference in hardness of the IMC product and the Mg base metal can cause brittleness in weld nugget edge (end of flat region). IMC formation and its effect will be discussed in more detail in next sections, which refer to temperature measurements and hardness evaluations, etc.

### 3.2. Interface Temperature Measurements

It is important be informed regarding rising temperature level during USW. The main factor affecting maximum process temperature ( $T_{max}$ ) is friction between the contacting surfaces. The friction is a result of shear force that is induced by transversely ultrasonic vibrations. As shown in Figure 3, temperature measurements have been conducted through the insertion of an accurate 0.5 mm diameter K-type thermocouple inside a notch at the centerline of joint in bottom plate. Temperature profiles that were obtained for different types of weldment combinations, as shown in Figure 7a and variation of  $T_{max}$  against distance from weld nugget center presented in the graphs of Figure 7b. Measurements were just performed on the strongest joint for each joint type. It means HP-USW under 1400 J for joint type A and 1100 J for joint type B.

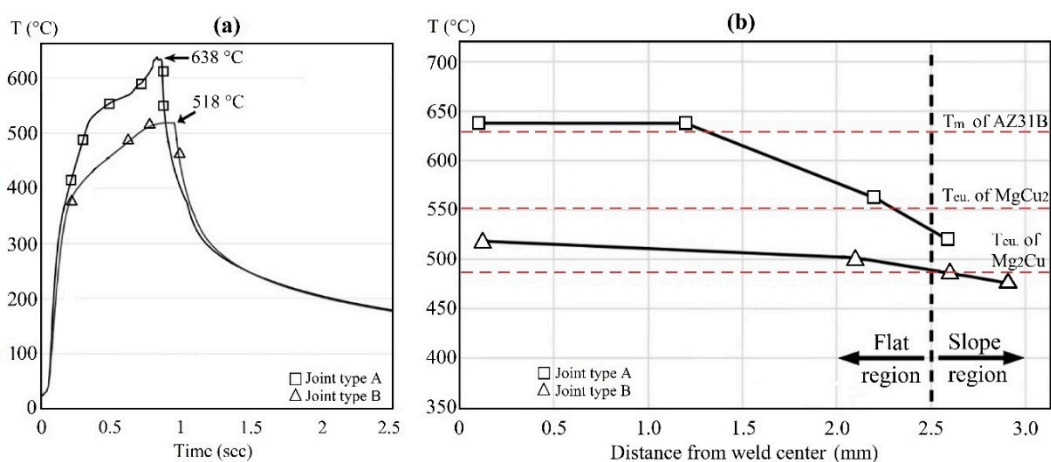


**Figure 7.** Interface temperature measurements for joint type A (1400 J) and joint type B (1100 J): (a) Comparative temperature profile for HP-USW of joint types A and B; (b) Maximum temperature of interface in different distances from weld center.

With looking at the temperature profiles of Figure 7a, it can be found that temperature firstly was increased from ambient temperature to a high level around 400 °C for joint B and 520 °C for joint A, sharply, just in a short duration of 0.2–0.3 s. Then, continuing of ultrasonic vibrations, led to completion of the bonding process, and temperature was increased to near the peak of  $T_{max}$  were observed. There is a clear difference between joint A and B at the maximum point, except the difference in  $T_{max}$  level. With using thin interlayer of Cu for joint type B, the peak temperature cycle in the curve flattened and  $T_{max}$  has longer persistence when compared to the joint type A. This can be predicated to the role of Cu that serves as a heat sink during the USW process. Without using the Cu interlayer (as in joint type A), the interface temperature increased and reached to  $T_{max}$  as a sharp peak with a duration of only 30 ms at the maximum point, and, while using the Cu interlayer besides lower energy, the peak shape somewhat flattened and was maintained near the  $T_{max}$  for a duration of 450 ms. After the  $T_{max}$  welding process is completed and ultrasonic vibrations stopped, weldment temperature decreased to near 300 °C very fast and then cooled down to ambient temperature, which continued for long time and nearly the same rate between two joint types.

Melting temperature ( $T_m$ ) for pure Mg is 650 °C, while  $T_m$  of AZ31B is 630 °C [28]. Knowing this, the  $T_{max}$  for joint type A (Power: 2450 W; Energy: 1400 J) was recorded at 638 °C, which is around the melting point of the AZ31B Mg alloy. However, referring to the microstructure observations that will be shown in Section 3.3 it is difficult to summarize that melting took place and it seems that the process

still occurs in the solid state. One reason might be cited to the short time of maximum temperature persistence with an appearance of a sharp peak in temperature profile. Additionally, looking at the temperature distribution in graphs of Figure 7b for joint type A represents  $T_{max}$  as accessible near the weld center and it quickly drops more than 120 °C in the half way of flat region. In Figure 7b, the melting point ( $T_m$ ) of AZ31B pointed out with a dashed line as a useful guide. The calculation of the surface area of joint type A where the temperature remains near the melting point of AZ31B proves that just 25% of weld nugget area can reach the maximum temperature (i.e., 4.6 mm<sup>2</sup> from nugget surface area exposed to  $T_{max}$ , against 19.6 mm<sup>2</sup> total nugget surface area in flat region). While, 75% of weld nugget area in joint type B fairly reach to maximum temperature and do not show a quick drop. Haddadi et al. [29] also evaluated the temperature drop from the nugget center to the weld edge and found that the peak temperature dropped by 50–130 °C at the weld edge for HP-USW of 0.93 mm thickness Al-6111.

In the other side, for joint type B (Power: 2450 W; Energy: 1100 J), the recorded  $T_{max}$  was 518 °C, which is apparent in Figure 7a, and the temperature distribution for this joint is presented in Figure 7b. In order to obtain a better understanding, two dashed lines that are related to critical temperatures in Mg-Cu binary system, as drawn in Figure 7b to show the situation of interfacial region. It can be found that most of interface flat region lies in the temperature values over Mg<sub>2</sub>Cu IMC formation eutectic temperature ( $T_{eu}$ ), which is 487 °C, but it cannot exceed  $T_{eu}$  of MgCu<sub>2</sub> IMC product, which is 552 °C. Therefore, it is predictable to achieve a kind of interfacial area that contains Mg<sub>2</sub>Cu as the main composition.

It is inferable that the Cu interlayer affects temperature distribution through improving the heat conductivity of interface. Copper has good electrical and heat conductivity and its thermal conductivity is four times larger than AZ31B Mg alloy (385 W/m-K for Cu; 96 W/m-K for Mg). Referring to this, the Cu effects on the interface to have a better heat distribution during the short time of process. Accordingly, with the matching graphs of Figure 7a,b for joint type B, it is clear that all parts of interface flat region have a chance of staying near maximum temperature for longer duration.

It is noteworthy to say that the Cu coating thin layer not only affected the thermal characteristics, but also the vibration behavior of interface. When using a Cu interlayer, USW impedance (a characteristic of vibration behavior) needs to set in lower levels to achieve proper resonance at the contact area of the two plates. In a research by Haddadi and Fadi [30], for dissimilar ultrasonic welding between steel and Al, they found that using a soft zinc coating on the steel surface altered the vibration behavior of the plate and the long sharp amplitude spike in the amplitude-time curve obviously decreased. They concluded that the surface condition of the steel sheet, which was confirmed by measurement of the net weld energy for each combination, affected the power delivery (when a fixed weld time was set). Furthermore, in that research, a eutectic reaction between Zn and Al led to a low melting point IMC reaction product that is molten under temperature rise that is caused by friction. The presence of this molten phase affected the amplitude of vibrations [30,31]. In the case of Mg-Cu, as it was explained, there is a eutectic point lower than process temperature that has the potential of making a molten phase and affecting the interface vibrational behavior. The effect of interlayer on impedance is also experimentally monitored through lap shear tensile force data before optimizing the energy effect on mechanical strength. At a constant USW energy and pressure, a change in impedance affected the process time and tip penetration depth and, accordingly, the optimized parameters that were used in experiments related to the effect of energy on maximum lap shear force.

### 3.3. Interface Characterization

#### 3.3.1. Light Microscopy Observation

Initial microstructure of base metal is depicted in Figure 8a, where it is related to the plate thickness intersection. Figure 8b depicts a schematic of raw material plate and observation surface for a better understanding. The microstructure of the as-rolled Mg base metal shown in Figure 8a included large

elongated grains inside the small equiaxed ones, with a mean grain size of  $3.5 \mu\text{m}$ . The deposited Cu interlayer had a random thickness instead of a uniform layer, as the average thickness of deposited Cu layer was measured to be  $2.5 \pm 1.0 \mu\text{m}$ .

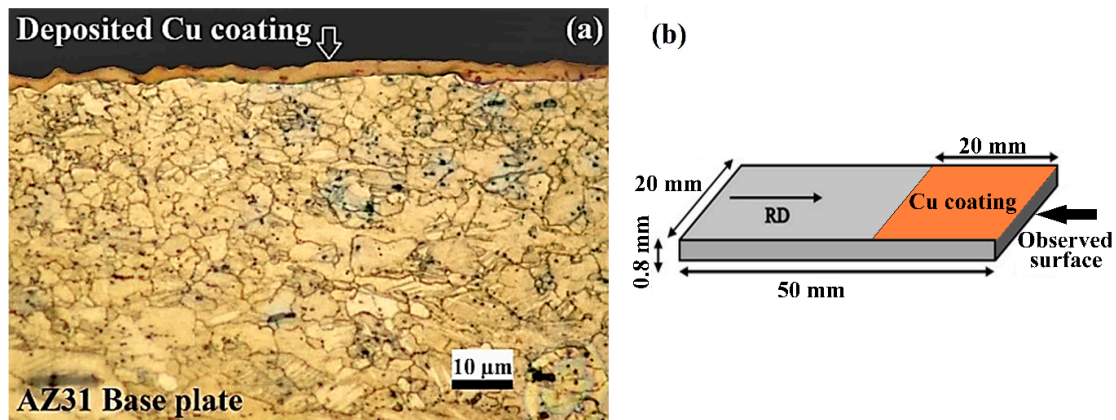


**Figure 8.** Light microscopy observation of AZ31 base metal with Cu coating, before USW (a) microstructure with Cu coating; (b) schematic of observed surface; (RD: Rolling direction).

Light microscopy evaluation on USW samples has been completed for two types of samples (A and B), but it was limited to strongest sample among all the samples in each type. The microstructure after ultrasonic welding is presented in Figure 9a,b for two joint types A and B, respectively.

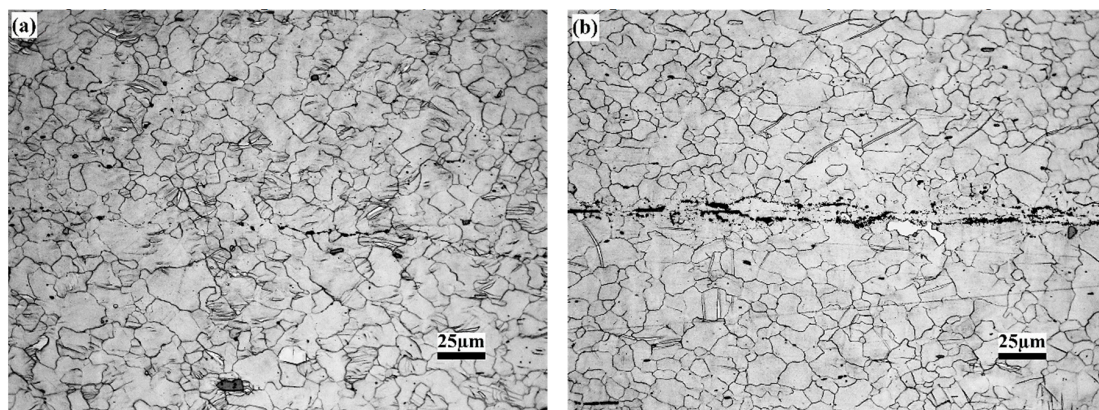


**Figure 9.** Light microscopy microstructure of interface flat region: (a) joint type A (1400 J); (b) joint type B (1100 J).

Firstly, through light microscopy microstructure for joint type B (Figure 9b) and comparing it with type A (Figure 9a), it was found that the use of copper coating resulted in a joint without discontinuity along the interface flat region. The observed interface showed a smooth flat interface. Some parts of the interface joined in bare contact between two Mg plates and it seems that the thin layer of Cu coating was scratched and removed due to scrubbing under high frequency ultrasonic vibrations and severe friction. As it was mentioned, the deposited Cu layer was a non-uniform coating layer and some parts were very thin when compared to total Cu layer (look at Figure 8a).

Afterwards, a comparison between microstructures before and after ultrasonic welding revealed amounts of grain growth and changing grain structure morphology. Grain size measurement for welded samples base metal was limited to nugget flat region inside a rectangular area of  $\pm 200 \mu\text{m}$  parallel to the interface centerline (except centerline and IMC layer). Morphology after ultrasonic welding for both joint types changed to larger grains with equiaxed structure, as grains were grown in the scale of about three times larger than initial base metal grain size. Figure 10 graphically summarizes the results.

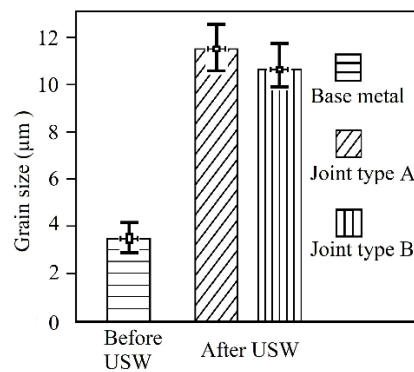


**Figure 10.** Comparison of base metal mean grain size before and after HP-USW for joint type A (1400 J) and joint type B (1100 J).

In joint type A, the mean grain size around the interface measured to be  $11.5 \mu\text{m} \pm 0.3$  in the average ( $11.2 \mu\text{m}$  for the top plate and  $11.8 \mu\text{m}$  for the bottom plate). It means that grain growth for this joint was in the scale of 3.3 times compared to initial base metal. For the joint type B, mean grain size around the interface was measured to be about  $10.7 \mu\text{m}$  ( $10.2 \mu\text{m}$  for the top plate and  $11.2 \mu\text{m}$  for the bottom plate). In the average, the mean grain size around the interface was about 7% smaller than the non-interlayered joint. This value also shows grain growth after ultrasonic welding that was about three times larger than initial base metal.

Grain growth after USW, has been frequently reported in previous researches in this field. For example, Macwan et al. [26] used USW for welding a rare-earth containing ZEK100 magnesium alloy in different USW energies 500–2000 J and observed that the average grain size in the NZ (nugget zone) increased from  $7.6$  to  $13.6 \mu\text{m}$ , while grains that were close to the weld interface were relatively coarser. The main effective parameter on grain growth is the enhanced temperature of joint interface due to friction. Accordingly, grain growth due to temperature rising can lead to soften the material, together with the fact that magnesium and its alloys have poor ductility and formability at room temperature, which can improve in elevated temperatures. Poor ductility was mainly related to their hexagonal closest packed (HCP) crystal structure and a lack of enough slip systems in low temperature due to highly anisotropic dislocation slip behavior. According to critical resolved shear stress (CRSS) analysis, only two independent slip systems (related to basal plane) are active in room temperature, while, based on Taylor/Von Mises criterion, at least five independent slip systems are needed for uniformly deformation without failure. As shown in Figure 7, the interface temperature increased to high levels around the melting point of AZ31B. At elevated temperatures, the formability of magnesium improves, owing to the activation of other non-basal slip systems, like secondary (c+a) pyramidal slip systems and easier movement and dislocation climbing [2,32,33]. Moreover, the process time in USW is very short and mentioning the role of high strain rates governing in USW that has an important effect on phenomena to occur in dynamic conditions is needed. Previously, other researchers discussed the role of dynamic recovery (DRV) and dynamic recrystallization (DRX) occurring in USW [9,27,34–37]. High strain rates in USW were reported to be in the scale of  $10^3 \text{ s}^{-1}$  [38]. Under high strain rate deformation, DRX occurs that leads to new equiaxed grain structure, followed by DRV under the effect of elevated temperature that affects on grain size to enlarging. Larger grains decrease the hardness of base metal that lead to softening the material. As vibrations periodically produce, this process can occur several times during the short cycle of the process. Material softening facilitates plastic deformation due to softer structure additionally to the activation of more slip systems in elevated temperature, as previously mentioned. Bakavos et al. described this procedure in more detail [9]. To ensure the effect of grain coarsening on softening the material and tracking the effect of IMC formation on interface mechanical properties, microhardness evaluations were done with a focus on the flat region, which presented in the next section.

### 3.3.2. Microhardness Evaluation

Hardness data after HP-USW obtained from corresponding area of flat region wherein the metallography grain size measurement was performed. Measurements verified the softening of weld base metal after USW, which is attributed to recovery in elevated temperature. The hardness of base metal before USW was 75 HV/10 gf/15 s (average of 10 points), while after the HP-USW of joint type A, it was decreased to 59.9 HV, shows about a 20% reduction in hardness. For joint type B, the average microhardness of base metal that was measured in nearly the same area as joint type A, out of IMC layer, was around 66.7 HV, which shows an 11% reduction in hardness when compared to the as-received material. According to grain size measurements, this evidence is reasonable, as that  $T_{max}$  for joint B was 120 °C lower than joint type A, hence the extent of softening is lower. Moreover, according to mean grain size evaluations in the previous section, the grain size of joint type B was 7% smaller than joint type A, which is in agreement with the hardness data achieved.

Hardness evaluation has also been performed on the IMC layer of joint type B, but it cannot assure real data, because the size of indentation effect was larger than the width of the IMC layer. Therefore, the acquired data is an average of the analyzed region, including an IMC layer and base metal. Accordingly, IMC containing region showed a clear increase in the hardness, as its average hardness was 105 HV/10 gf/15 s. This value is 40% more than raw material hardness. The hardness data reported by other researchers on thick IMC layer between Mg and Cu also confirmed an increase in interface hardness. For example, Macwan et.al. reported a sharp increase in hardness at the interface of ultrasonically welded AZ31 to Cu in the scale of 278 HV as related to the Mg<sub>2</sub>Cu intermetallic compound [15]. By the way, the high hardness of interfacial region is evidence of a eutectic reaction and the formation of IMC products.

### 3.3.3. Electron Microscopy Analysis

Magnesium etchant that used in metallography trials cannot simultaneously attack pure Cu, and, if some parts of Cu remained unreacted after USW, it is distinctly recognizable with a red tint in light microscopy photos, as that visible in Figure 8a. Meanwhile, interfacial layer in joint type B has a black and white appearance, which affirms the complete reaction of Cu and the formation of IMC products, alongside microhardness findings. Accordingly, for the better interface characterization of joint type B, more precise analysis methods based on electron microscopy are needed.

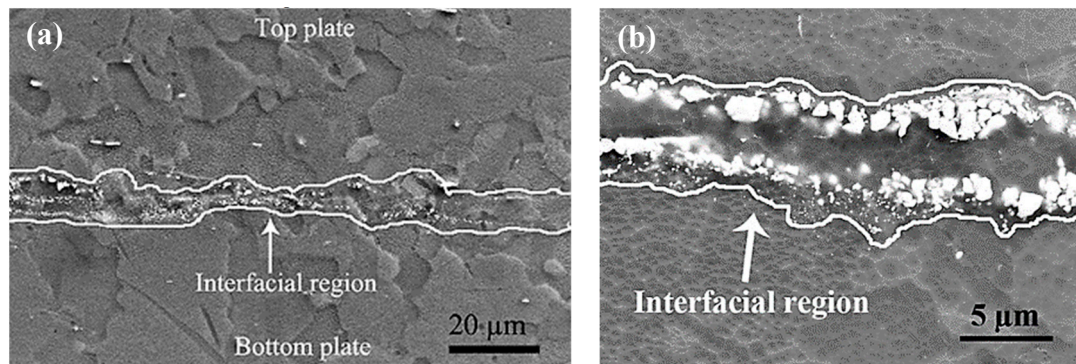
### SEM Interface Observation

Figure 11a,b present the SEM observation on joint type B. Two white lines were graphically added inside the photos to create better perception regarding the interfacial region. The total thickness of Cu deposited layer before USW was only about 2.5 μm, but the affected interfacial region is much wider than the initial thickness of the Cu coating interlayer and it has an average width of around 9 μm, i.e., near four times larger than the initial thickness of the Cu coating. This is evidence of diffusion during the eutectic reaction.

This region can be seen in more detail at higher magnification, as in Figure 11b. The main reaction products are visible as discrete white particles, instead of a continuous layer. Apart from the composition of these particles, the dispersion of such hard IMC products inside a soft matrix of AZ31B base metal performs a composite like structure at the interface that can participate in the strengthening of the welded joint. Previously, in Section 3.1 it was reported that failure occurred in the pull out mode from the nugget edge walls. It means that crack initiation was not introduced from the flat region interface and it is a sign of strong sound joint.

The occurrence observed in Figure 11b specifies that reaction products were found in farther distances, like diffusion in base metal. This can be stimulated under the effect of enhanced temperature and ultrasonic vibrations. As it was noticed before, the interface temperature rises to over  $T_{eu}$  of Mg<sub>2</sub>Cu,

which predicts the presence of a liquid phase that is able to diffuse through material imperfections, like grain boundaries. The EBSD results in next section will show this matter in more detail.



**Figure 11.** Interface SEM observation of joint type B (1100 J), (a) low magnification; (b) high magnification.

Interdiffusion of Mg and Cu in steady state conditions were studied before and discussed briefly in the introduction, but the lack of consensus in diffusion data makes diffusion behavior difficult to interpret. For example, activation energy data for the diffusion of Cu in Mg or vice versa are not compatible in different studies. Nonaka et al. [13] studied the reaction diffusion in Mg-Cu diffusion couple between 410–475 °C and observed that Kirkendall markers shifted towards the Cu-rich side, so they suggested that the diffusion of Cu is faster than Mg and they measured the activation energy of  $Mg_2Cu$  as 156 kJ/mole. Additionally, the growth rate of  $Mg_2Cu$  was much larger than  $MgCu_2$ . Other research by Dai et al. [14] in nearly the same conditions (400–460 °C) similarly found that, at all examined temperatures, two intermetallic layers formed between Mg and Cu, including the  $Mg_2Cu$  layer close to Mg side and  $MgCu_2$  in contact with Cu side. The  $Mg_2Cu$  layer (with almost no solubility) was much thicker than  $MgCu_2$ . They also measured the activation energies for both IMCs that resulted in a lower value for  $Mg_2Cu$  (139 kJ/mole) when compared to  $MgCu_2$  (147 kJ/mole). As it is clear, their data were a little different from reference [13]. The other important information that was obtained in reference [14] was related to activation energies for diffusion of Mg in Cu (139 kJ/mole) and Cu in Mg (164 kJ/mole), which imply different interdiffusion behavior when compared to reference [13].

However it is not the objective of current study to derive the diffusion data and, as was mentioned before, the USW process is more complicated than the original diffusion couples in steady state static conditions, due to high strain rates and vibrations in short time (less than 1 s for USW when compared to 24–72 h in reaction diffusion), but some findings, such as formation priority and layer thickness of  $Mg_2Cu$ , are in relative concurrency.

The formation of these two reaction products is based on a simple Mg-Cu system, while, in the presence of major alloying elements of AZ31B, the synthesis of other by-products also is expectable. For example, the Al content in AZ31B Mg alloy can contribute to form non-stoichiometric binary or ternary IMC products, together with Cu.

#### EBSD Analysis

For better clarification of the interfacial structure, EBSD analysis observations on the strongest joint of type B are done and taken in Figure 12. Figure 12a–c shows the interface area in different magnifications prepared by EBSD phase map (12a) and inverse pole figure map (12b,c).

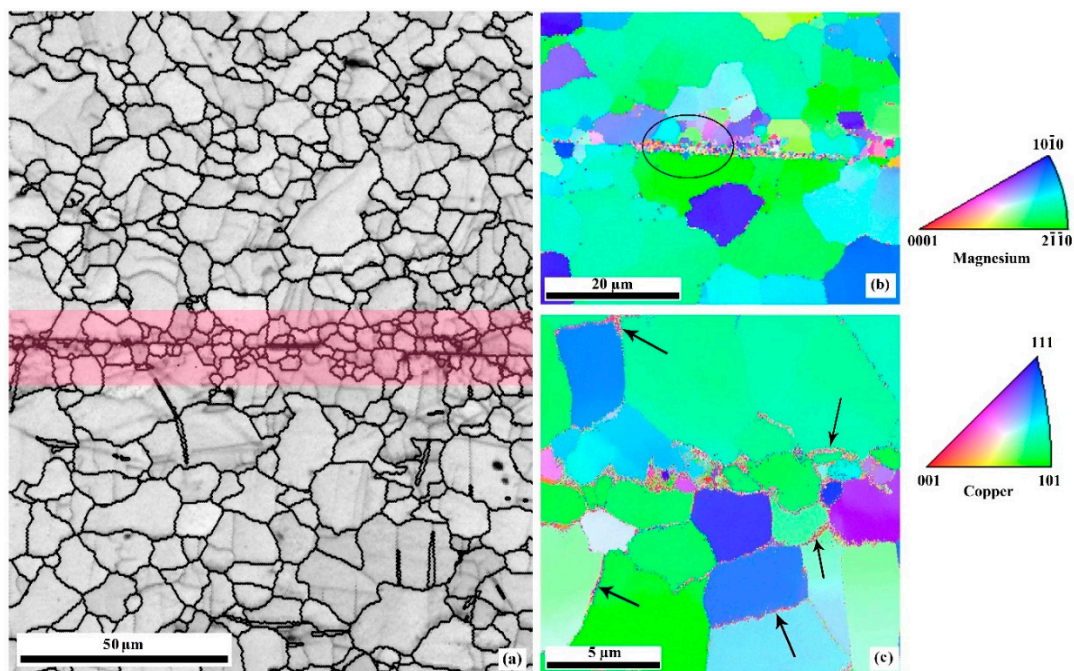


**Figure 12.** EBSD analysis on joint type B (1100 J), for (a) low magnification phase map with grain boundaries, (b), and (c) IPF colored map of interface in different magnifications.

Figure 12a illustrates a low magnification phase map of the interfacial region. A chain of base metal relatively fine grains (in comparison to large grains of base metal after HP-USW), adjacent to the interface centerline, is distinguishable. For better understanding, this region was graphically covered with a pink mask. Other researchers observed this type of fine-grained structure and they called it a “necklace-like” grain structure. The main effective parameter to produce this chain of smaller grains is occurrence of DRX, because, among interfacial area, this region suffers higher strain rates and plastic deformation that were caused due to friction between two faying surfaces [9,27,29]. Other regions far from the interface, as described in 3.3.1, shows an equiaxed grain structure, where the size of grains is larger than the base metal before welding. The IMC containing layer in Figure 12a has a dark feature at the interface centerline. Since that IMC grains are ultrafine, the grain boundaries covered the face of grains to be darkened. With looking overall at the interface in the metallography and EBSD photos, it can be found that some regions lost the Cu coating because of high frequency vibrations and friction. Moreover, the deposited layer thickness is not uniform in various parts of interface; thereupon, the width of interfacial reaction layer differs part by part. There is a direct bare contact between top plate and bottom plate without the presence of an interlayer in some regions of the interface.

In Figure 12b, the IMC reaction products are visible as fine grains that are distributed along the interface and neighborhood areas. The noticed region inside an oval in Figure 12b is an IMC-containing area at the interface, which is shown in more detail in Figure 12c. Figure 12c shows that a portion of ultrafine particles that are probably molten during HP-USW diffused through the grain boundaries of base metal to farther distances, in addition to the presence at the interface centerline. Some of diffused particles were typically pointed with black arrows to have better perception. With use of EBSD computer software, it was found that the diffused particles are Cu-containing reaction products. More accurate identification of particles was made possible through EPMA and TEM analysis.

Consequently, according to EBSD observations, good evidences were obtained for grain size strengthening based on well-known “Hall-Petch” equation, as supported by fine grains of base metal around the interface and ultrafine grains of hard IMC particles distributed in interfacial region.

### EPMA Analysis

EPMA analysis also accomplished for joint type B and is presented in Figure 13. This elemental map analysis on joint type B indicated high levels of Mg at the interface and smaller levels of Cu and Al. The elemental map of Zn (not presented here) included a uniform distribution of it in all areas as a low percentage trace element.

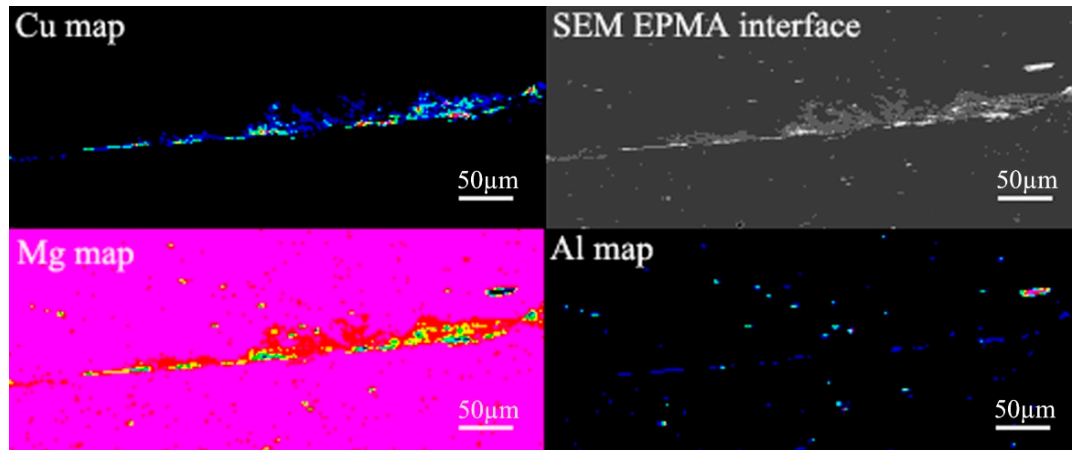


**Figure 13.** EPMA analysis on joint type B (1100 J) interface: Map of Mg, Cu and Al.

Two main regions are recognizable while looking at three elemental EPMA maps in Figure 13, and comparing them with SEM-EPMA interface photo. The main region is an area around the interface, wherein maps of Mg and Cu exhibit good overlapping together. Mg is prevalent in this region, and Cu is in a lower concentration that predicts a composition rich in Mg with lower content of Cu. As it was explained before, there are two main compositions in the binary phase diagram of Mg-Cu, including  $Mg_2Cu$  and  $MgCu_2$ . Keeping this in mind, it should be again noticed that the maximum interface temperature obtained for this joint was 518 °C (see Figure 7), which is over  $T_{eu}$  of  $Mg_2Cu$  and lower than that for  $MgCu_2$ , hence it can be suggested that the main area around the interface is composed of  $Mg_2Cu$  intermetallic compound.

Another interfacial region recognized in the centerline of the interface, consisted of a composition containing Al, Mg, and Cu. It seems that the resolution of EPMA analysis is not enough to identify the reaction product in the centerline. Therefore, TEM analysis also done on this region.

### TEM Interface Analysis

The Al-containing region at the interface centerline that explored with EPMA analysis has been studied by TEM. Samples for TEM were extracted from the center of interface flat region in a direction similar to SEM-EPMA samples. Ultrafine particles that distributed inside an Mg substrate were found in this region and DP (diffraction pattern) analysis on them are shown in Figure 14a,b.

Based on measurements completed on DP's, it was found that the substrate (Figure 14a) shows crystal structure that precisely matches the HCP structure of magnesium. The DP of particles indicated a material with lattice spacing values of 0.42 nm; 0.44 nm; and, 1.68 nm. According to library data, the closest match is a ternary composition of type  $MgCu_xAl_y$ . Based on Buhler (1998) and Mel'nik (1981), the composition of  $MgCu_{1.1}Al_{0.9}$  4H (hp24, P63/mmc), with cell parameters of 0.51 nm; 0.51 nm; and, 1.676 nm, that is a Friauf-Laves phase C36 is the nearest estimation [39,40]. Change in indices  $x$  and  $y$  were attributed to the non-stoichiometry intermetallic compounds. Other products in this ternary system do not match with our findings.

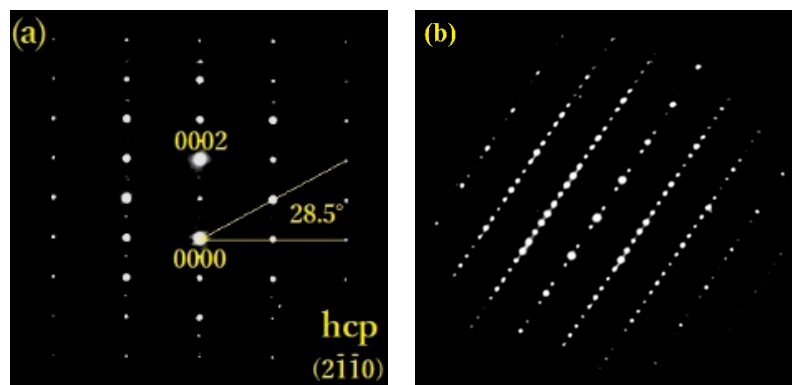


**Figure 14.** TEM analysis on joint type B (1100 J); diffraction pattern (DP) of (a) Mg matrix; (b) intermetallic compound (IMC) particles, at the interface centerline region.

#### 4. Conclusions

AZ31B Mg alloy joints welded through HP-USW, with and without the use of Cu coating interlayer, and the following main results concluded:

1. Microstructure observations on interface, together with high mechanical strength and nugget pull-out fracture, revealed good weldability of the Cu interlayered joint.
2. Highest strength for interlayered joints was achieved in 20% lower USW energy, as compared to joints without the interlayer.
3. The microstructure of base metal after USW, converted to enlarged equiaxed grains with grain growth in the scale of three times larger than initial value, which is attributed to enhanced temperature, alongside high strain rates of HP-USW under the effect of DRX and DRV phenomena.
4. Temperature data, alongside EPMA analysis, suggested the formation of  $Mg_2Cu$  as the main IMC product around the interface. Additionally, EBSD analysis showed the diffusion and spreading of IMC's to farther the distances from the interface centerline, especially through grain boundaries.
5. Proper strength of the interlayered joint is cited to the presence of fine grains of base metal adjacent to the interface and the dispersion of ultrafine hard IMC reaction products inside the soft matrix of Mg.
6. TEM analysis declared that the Al-containing reaction product that is found in the interface centerline is a composition of type  $MgCu_xAl_y$ , which is a Friauf–Laves phase.

**Author Contributions:** Experiments conceived and designed by A.B. and C.I.; Manuscript wrote by A.B.; Supervision and TEM analysis, C.I.; Consultant and EBSD analysis, S.S.; Consultant and performing coating by vapor deposition, S.T.

**Funding:** This research received no external funding.

**Conflicts of Interest:** The authors declare no conflict of interest.

#### References

1. Avedesian, M.M.; Baker, H. *ASM Specialty Handbook: Magnesium and Magnesium Alloys*; ASM International: Novolty, OH, USA, 1999; ISBN 978-0-87170-657-7.
2. Ropp, R.C. *Encyclopedia of the Alkaline Earth Compounds*; Elsevier: Oxford, UK, 2013; ISBN 978-0-444-59550-8.
3. Harooni, M.; Kovacevic, R. Laser Welding of Magnesium Alloys: Issues and Remedies. In *Magnesium Alloys*; Aliofkhaezrai, M., Ed.; IntechOpen: London, UK, 2017; Available online: <https://www.intechopen.com/books/magnesium-alloys> (accessed on 1 April 2019).
4. Czerwinski, F. Welding and Joining of Magnesium Alloys. In *Magnesium Alloys—Design, Processing and Properties*; InTech: Rijeka, Croatia, 2011; pp. 469–490, ISBN 978-953-307-520-4.

5. Haddadi, F. Ultrasonic Spot Welding. In *Advanced Manufacturing Technologies Modern Machining, Advanced Joining, Sustainable Manufacturing*; Gupta, K., Ed.; Springer International Publishing AG: Cham, Switzerland, 2017; pp. 185–209, ISBN 978-3-319-56098-4.
6. Wang, T.; Shukla, S.; Gwalani, B.; Komarasamy, M.; Reza-Nieto, L.; Mishra, R.S. Effect of reactive alloy elements on friction stir welded butt joints of metallurgically immiscible magnesium alloys and steel. *J. Manuf. Process.* **2019**, *39*, 138–145. [[CrossRef](#)]
7. Edison, K.G. Ultrasonic metal welding. In *New Developments in Advanced Welding*; Ahmed, N., Ed.; Woodhead Publishing Ltd.: Cambridge, UK, 2005; pp. 241–269, ISBN 978-1-85573-970-3.
8. Devine, J. Ultrasonic Welding. In *ASM Metals Handbook*; Lienert, T.J., Babu, S.S., Siewert, T.A., Acoff, V.L., Eds.; ASM International: Materials Park, OH, USA, 2011; Volume 6A, pp. 725–730, ISBN 978-1-61503-133-7.
9. Bakavos, D.; Prangnell, P.B. Mechanisms of joint and microstructure formation in high power ultrasonic spot welding 6111 aluminum automotive sheet. *Mater. Sci. Eng. A* **2010**, *527*, 6320–6334. [[CrossRef](#)]
10. Fujii, H.T.; Goto, Y.; Sato, Y.S.; Kokawa, H. Microstructural evolution in dissimilar joint of Al alloy and Cu during ultrasonic welding. *Mater. Sci. Forum* **2014**, *783–786*, 2747–2752. [[CrossRef](#)]
11. Sanga, B.; Wattal, R.; Nagesh, D.S. Mechanism of joint formation and characteristics of interface in ultrasonic welding: Literature review. *Period. Eng. Nat. Sci. (PEN)* **2018**, *6*, 107–119. [[CrossRef](#)]
12. Jahn, R.; Cooper, R.; Wilkosz, D. The effect of anvil geometry and welding energy on microstructures in ultrasonic spot welds of AA6111-T4. *Metall. Mater. Trans. A* **2007**, *38*, 570–583. [[CrossRef](#)]
13. Nonaka, K.; Sakazawa, T.; Nakajima, H. Reaction diffusion in Mg-Cu system. *Mater. Trans. JIM* **1995**, *36*, 1463–1466. [[CrossRef](#)]
14. Dai, J.; Jiang, B.; Zhang, J.; Yang, Q.; Jiang, Z.; Dong, H.; Pan, F. Jiang binary system. *J. Phase Equilib. Diffus.* **2015**, *36*, 613–619. [[CrossRef](#)]
15. Macwan, A.; Chen, D.L. Microstructure and mechanical properties of ultrasonic spot-welded copper to magnesium alloy joints. *Mater. Des.* **2015**, *84*, 261–269. [[CrossRef](#)]
16. Elthalabawy, W.M.; Khan, T.I. Eutectic bonding of austenitic stainless steel 316L to magnesium alloy AZ31 using copper interlayer. *Int. J. Adv. Manuf. Technol.* **2011**, *55*, 235–241. [[CrossRef](#)]
17. Elthalabawy, W.; Khan, T.I. Liquid phase bonding of 316L stainless steel to AZ31 magnesium alloy. *J. Mater. Sci. Technol.* **2011**, *27*, 22–28. [[CrossRef](#)]
18. Panteli, A.; Robson, J.D.; Chen, Y.C.; Prangnell, P.B. The effectiveness of surface coatings on preventing interfacial reaction during ultrasonic welding of aluminum to magnesium. *Metall. Mater. Trans. A* **2013**, *44*, 5773–5781. [[CrossRef](#)]
19. Panteli, A.; Robson, J.D.; Brough, I.; Prangnell, P.B. The effect of high strain rate deformation on intermetallic reaction during ultrasonic welding aluminium to magnesium. *Mater. Sci. Eng. A* **2012**, *556*, 31–42. [[CrossRef](#)]
20. Panteli, A.; Chen, Y.C.; Strong, D.; Zhang, X.; Prangnell, P.B. Optimization of aluminium to magnesium ultrasonic spot welding. *JOM* **2012**, *64*, 414–420. [[CrossRef](#)]
21. Patel, V.K.; Bhole, S.D.; Chen, D.L. Improving weld strength of magnesium to aluminium dissimilar joints via tin interlayer during ultrasonic spot welding. *Sci. Technol. Weld. Join.* **2012**, *17*, 342–347. [[CrossRef](#)]
22. Patel, V.K.; Bhole, S.D.; Chen, D.L. Ultrasonic spot welding of lightweight alloys. In Proceedings of the 13th International Conference on Fracture, Beijing, China, 16–21 June 2013.
23. Liu, J.; Cao, B.; Yang, J. Effects of vibration amplitude on microstructure evolution and mechanical strength of ultrasonic spot welded Cu/Al joints. *Metals* **2017**, *7*, 471. [[CrossRef](#)]
24. Mezbahul-Islam, M.; Mostafa, A.M.; Medraj, M. Essential magnesium alloys binary phase diagrams and their thermochemical data. *J. Mater.* **2014**, *2014*, 704283. [[CrossRef](#)]
25. Peng, H.; Chen, D.L.; Bai, X.F.; She, X.W.; Li, D.Y.; Jiang, X.Q. Ultrasonic spot welding of magnesium to aluminum alloys with a copper interlayer: Microstructural evolution and tensile properties. *J. Manuf. Process.* **2019**, *37*, 91–100. [[CrossRef](#)]
26. Macwan, A. Ultrasonic Spot Welding of Similar and Dissimilar Alloys for Automotive Applications. Ph.D. Thesis, Ryerson University, Toronto, ON, Canada, 2016.
27. Peng, H.; Chen, D. Microstructure and mechanical properties of an ultrasonic spot welded aluminum alloy: The effect of welding energy. *Materials* **2017**, *10*, 449. [[CrossRef](#)] [[PubMed](#)]
28. Brandes, E.A.; Brook, G.B. *Smithells Light Metals Handbook*; Butterworth-Heinemann: Oxford, UK, 1998; ISBN 978-0-7506-3625-4.

29. Haddadi, F.; Tsivoulas, D. Grain structure, texture and mechanical property evolution of automotive aluminum sheet during high power ultrasonic welding. *Mater. Charact.* **2016**, *118*, 340–351. [[CrossRef](#)]
30. Haddadi, F.; Fadi, A. The effect of interface reaction on vibration evolution and performance of aluminum to steel high power ultrasonic spot joints. *Mater. Des.* **2016**, *89*, 50–57. [[CrossRef](#)]
31. Derks, P.L.L.M. Parameters that influence the ultrasonic bond quality. *Electron. Compon. Sci. Technol.* **1983**, *10*, 269–275. [[CrossRef](#)]
32. Al-Samman, T.; Gottstein, G. Dynamic recrystallization during high temperature deformation of magnesium. *Mater. Sci. Eng. A* **2008**, *490*, 411–420. [[CrossRef](#)]
33. Itakura, M.; Kaburaki, H.; Yamaguchi, M.; Tsuru, T. Novel cross-slip mechanism of pyramidal screw dislocations in magnesium. *Phys. Rev. Lett.* **2016**, *116*, 225501. [[CrossRef](#)]
34. Patel, V.K.; Bhole, S.D.; Chen, D.L. Influence of ultrasonic spot welding on microstructure in a magnesium alloy. *Scr. Mater.* **2011**, *65*, 911–914. [[CrossRef](#)]
35. Xiea, J.; Zhua, Y.; Bianc, F.; Liud, C. Dynamic recovery and recrystallization mechanisms during ultrasonic spot welding of Al-Cu-Mg alloy. *Mater. Charact.* **2017**, *132*, 145–155. [[CrossRef](#)]
36. Shimizu, S.; Fujii, H.T.; Sato, Y.S.; Kokawa, H.; Sriraman, M.R.; Babu, S.S. Mechanism of weld formation during very-high-power ultrasonic additive manufacturing of Al alloy 6061. *Acta Mater.* **2014**, *74*, 234–243. [[CrossRef](#)]
37. Fujii, H.T.; Sriraman, M.R.; Babu, S.S. Quantitative evaluation of bulk and Interface microstructures in Al-3003 alloy builds made by very high power ultrasonic additive manufacturing. *Metall. Mater. Trans. A* **2011**, *42*, 4045–4055. [[CrossRef](#)]
38. Gunduz, I.E.; Ando, T.; Shattuck, E.; Wong, P.Y.; Doumanidis, C.C. Enhanced diffusion and phase transformations during ultrasonic welding of zinc and aluminum. *Scr. Mater.* **2005**, *52*, 939–943. [[CrossRef](#)]
39. Buhler, T.; Fries, S.G.; Spencer, P.J.; Lukas, H.L. A Thermodynamic assessment of the Al-Cu-Mg ternary system. *J. Phase Equilib.* **1998**, *19*, 317–333. [[CrossRef](#)]
40. Mel'nik, E.V.; Kinzhibalo, V.V. Investigation of the Mg-Al-Cu and Mg-Ga-Cu systems from 33.3 to 100 at. % Mg. *Russ. Metall.* **1981**, *3*, 154–158.



© 2019 by the authors. Licensee MDPI, Basel, Switzerland. This article is an open access article distributed under the terms and conditions of the Creative Commons Attribution (CC BY) license (<http://creativecommons.org/licenses/by/4.0/>).